Fatigue life analysis of fiber reinforced concrete with a fracture mechanics based model

Takashi Matsumoto [a,*], Victor C. Li [b]

[a] *Department of Civil Engineering, University of Tokyo, 7-3-1 Hongo, Bunkyo-ku, Tokyo 113-8656, Japan*
[b] *Advanced Civil Engineering Materials Research Laboratory, Department of Civil and Environmental Engineering, University of Michigan, Ann Arbor, MI 48109-2125, USA*

Abstract

Fatigue life of fiber reinforced concrete (FRC) is theoretically analyzed with a fracture mechanics based model. The model accounts for the effect of cycle-dependent crack bridging properties in FRCs and predicts the number of cycles to failure defined by final fracture subsequent to stable fatigue crack growth in Mode I. The resulting theoretical S–N diagram was compared with experimental data reported in literature. The general agreement supports the validity of the current model, and reveals that cycle-dependent degradation of crack bridging controls fatigue life of FRCs. S–N diagrams are essential for material evaluation and structural design, and the model establishes the link between material structure and S–N diagram in an explicit manner, while the conventional stress-life approach realizes the link in an empirical manner. © 1999 Elsevier Science Ltd. All rights reserved.

Keywords: Fatigue; Fiber reinforced concrete; Fracture Mechanics

1. Introduction

Development of high fatigue resistant FRCs can contribute to the successful development and maintenance of civil infrastructures. FRCs have been applied to civil infrastructure facilities such as pavements, overlays, bridge deck overlays, railroad sleepers, and industrial floors [1–5]. These facilities have to be maintained in a good service condition, because of their importance to society in many ways, but these facilities may deteriorate due to their exposure to fatigue condition: heavy and frequent loads. Deterioration of highly developed civil infrastructures including these facilities causes serious problems, and maintenance and rehabilitation costs accumulate as civil infrastructures are further developed. To avoid uncontrollable deterioration of civil infrastructures, FRCs are required to be both high in fatigue resistance and low in life-cycle cost so that FRCs can fulfill the expected service life of facilities in a cost-efficient manner. Development of high fatigue resistant FRCs has to satisfy the requirements, and this is made feasible when based on the understanding of mechanisms and microstructural parameters that are responsible for fatigue of FRCs.

The development of high fatigue resistant FRCs has relied mainly on an empirical trial and error approach, with experimental determination of an S–N diagram being performed on an FRC beam. S–N diagrams are essential for two reasons: material evaluation and structural design. With an S–N diagram, a new material can be evaluated in comparison to existing materials, and a structure can be designed with allowable stress level under given fatigue life. However, this approach is not efficient due to two disadvantages. First, it requires time-consuming experimental data collection to obtain an S–N diagram. Second, it takes a trial and error approach for the development purpose due to the lack of understanding of mechanisms and microstructural parameters responsible for fatigue of FRCs. These two disadvantages should be removed so that the efficient development of high fatigue resistant FRCs can be achieved, while the importance of S–N diagrams is recognized. A theoretical S–N diagram based on the understanding of mechanisms and microstructural parameters responsible for fatigue of FRCs would increase the efficiency of the development.

---

* Corresponding author. Tel.: +81-3-3812-2111; fax: +81-3-3812-4977; e-mail matsumoto@civil.t.u-tokyo.ac.jp

Theoretical S–N diagrams of FRCs can be generated with a fracture mechanics based model that showed agreement with experimental data in three distinct stages of fatigue crack growth of an FRC [6]. The model predicts the number of cycles to failure which is defined by final failure subsequent to fatigue crack growth, accounting for the effect of cycle-dependent crack bridging, and it is expressed explicitly in terms of microstructural parameters of FRCs (for example, fiber length, fiber diameter, fiber modulus, fiber volume fraction, and interfacial bond strength). In this paper, the theoretical S–N diagram of four different FRCs has been obtained with the model presented in Li and Matsumoto [6]. It shows that a simple assumption pertaining to the cycle-dependent degradation of crack bridging explains a wide range of experimental results reported in the literature and that the modification of fiber-matrix interface may lead to fatigue life improvement.

2. Fracture mechanics based fatigue life model

The fracture mechanics based fatigue model of randomly distributed discontinuous fiber composites developed by Li and Matsumoto [6] is summarized in this section. Details of the model can be found in Li and Matsumoto [6], Matsumoto and Li [7], and Wu et al. [8]. The fatigue life model is based on fracture mechanics of fatigue crack growth of FRCs. FRCs fail in fatigue when final unstable fracture takes place subsequent to stable crack growth under fatigue loading. Thus, fatigue life of FRCs is defined by the number of cycles to final failure and, in turn, is controlled by fatigue crack growth behavior. Fatigue crack growth is governed by three factors: matrix fatigue crack growth law, crack bridging, and cycle-dependent degradation of crack bridging (Fig. 1). These three factors are reviewed below.

2.1. Matrix fatigue crack growth law

Matrix fatigue crack growth law for cementitious materials has been observed to obey a Paris law type equation [9–13]. Paris law presents the relation between crack growth rate and crack tip stress intensity factor amplitude as

$$\frac{\mathrm{d}a}{\mathrm{d}N} = C\left(\Delta K_{\mathrm{tip}}\right)^n, \tag{1}$$

where a is the crack length, N the number of load cycles, C Paris constant, ΔK_{tip} the crack tip stress intensity factor amplitude, and n the Paris constant [14]. Thereby, the current number of load cycles, N, at a given crack length, a, can be obtained by
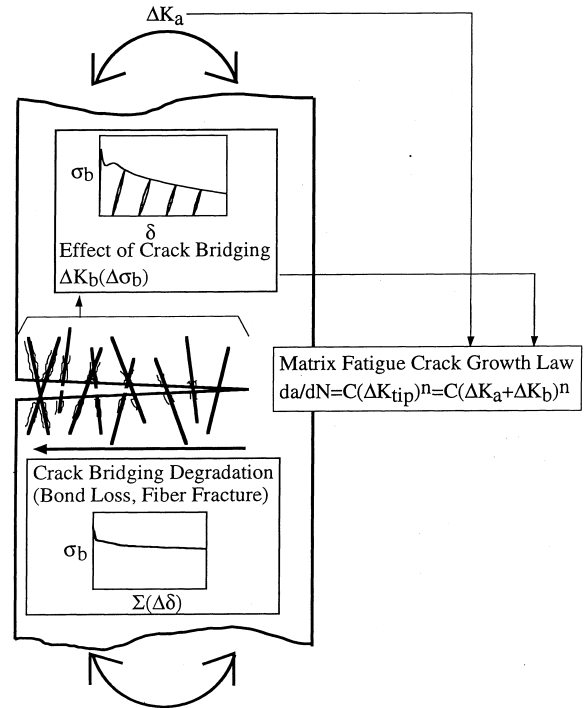

Fig. 1. Fatigue damage on material constituents.

$$N = \int_{a_{\mathrm{i}}}^{a} \frac{1}{C\left(\Delta K_{\mathrm{tip}}\right)^n} \,\mathrm{d}a, \tag{2}$$

where a_{i} is the initial crack length.

Fatigue life, N_{f}, is defined by final unstable fracture subsequent to fatigue crack growth and is obtained by calculating the number of load cycles spent for growing the crack from the initial length, a_{i}, to the final length, a_{f}. This final unstable fracture condition is met when crack tip stress intensity factor surpasses matrix fracture toughness and is simply given by

$$K_{\max} = K_{\mathrm{c}}, \tag{3}$$

where $K_{\max}$ is the crack tip stress intensity factor at maximum load level and K_{c} matrix fracture toughness. $K_{\max}$ is a function of body geometry, loading mode, crack bridging, and crack configuration, so the condition determines the final crack length, a_{f}, at fracture failure when other variables are given.

Hence, fatigue life can be computed, if ΔK_{tip} and $K_{\max}$ are obtained for a given FRC for a given body geometry and loading mode. ΔK_{tip} and $K_{\max}$ can be determined using similar procedures, and only the steps to obtain ΔK_{tip} are summarized below. The crack tip stress intensity factor amplitude, ΔK_{tip}, of FRCs is attributed to external applied loading and crack bridging, so ΔK_{tip} can be decomposed into two parts:

$$\Delta K_{\mathrm{tip}} = \Delta K_{\mathrm{a}} + \Delta K_{\mathrm{b}}, \tag{4}$$

where ΔK_a is the stress intensity factor amplitude due to external applied loading and ΔK_b the stress intensity factor amplitude due to crack bridging. ΔK_a for a beam in flexural bending that has a crack on the tension face is given by

$$\Delta K_a = 2 \int_0^a G(x, a, w) \Delta \sigma_a(x) \mathrm{d}x, \tag{5}$$

where w is the beam depth, $\Delta \sigma_a(x) = \Delta \sigma_0 (1 - 2x/w)$ (linear gradient for bending), $\Delta \sigma_0 =$ applied external flexural stress amplitude, which is the difference between σ_{max} the maximum stress level and σ_{min} the minimum stress level, and x is measured from the tension face of the beam [15,16]. $G(x, a, w)$ is a weight function that represents the contribution of a unit force on the crack surface to the crack tip stress intensity factor and is specific to body geometry and crack configuration [15,16]. Similarly, ΔK_b is a function of the relation between the crack bridging stress amplitude, $\Delta \sigma_b$, and the crack opening displacement amplitude, $\Delta \delta$, (hereafter referred to as the cyclic bridging law) and is given by

$$\Delta K_b = -2 \int_0^a G(x, a, w) \Delta \sigma_b(\Delta \delta(x)) \mathrm{d}x, \tag{6}$$

where $\Delta \sigma_b(\Delta \delta)$ is the cyclic bridging law and $\Delta \delta(x)$ the crack opening displacement amplitude at a point, x, on the crack surface.

The computation of ΔK_{tip} and K_{max} requires a numerical scheme to solve an integral equation on crack opening displacement amplitude, $\Delta \delta(x)$, and crack opening displacement at maximum load level, $\delta_{max}(x)$, at a position, x, on the crack surface, respectively. The integral equation on $\Delta \delta(x)$ is given by

$$\frac{\Delta \delta(x)}{2} = \frac{4}{E} \int_x^a \left\{ \int_0^{a'} G(x', a', w)[\Delta \sigma_a(x') \right. $$
$$\left. - \Delta \sigma_b(\Delta \delta(x'))]\mathrm{d}x' \right\} G(x', a, w) \mathrm{d}a'. \tag{7}$$

This equation is transformed into a matrix equation on $\Delta \delta(x(i))$ at grid points, $(x(i), i = 0, \ldots, m)$, where the solution is equivalent to that of the original integral equation with the use of cubic spline integration over the grid points. Details on the numerical scheme can be found in Cox and Marshall [16].

2.2. Cyclic bridging law

Crack bridging in FRCs is exerted by fibers and aggregates. Thus, the cyclic bridging law, $\Delta \sigma_b(\Delta \delta)$, is given by the superposition of crack bridging stress-crack

opening displacement relation due to fibers and aggregates under cyclic loading:

$$\Delta \sigma_b = \Delta \sigma_f + \Delta \sigma_m, \tag{8}$$

where $\Delta \sigma_f$ is the fiber bridging stress change under cyclic loading and $\Delta \sigma_m$ the aggregate bridging stress change under cyclic loading.

Cyclic bridging law due to fibers, $\Delta \sigma_f(\Delta \delta)$, is based on the micromechanics of fiber bridging under cyclic loading. The expression of $\Delta \sigma_f(\Delta \delta)$ is summarized in Appendix A, and more details can be found in Wu et al. [8] and Matsumoto and Li [7]. The normalized cyclic bridging law due to fibers can be represented by

$$\Delta \tilde{\sigma}_f = \text{function}\left(\Delta \tilde{\delta}, \tilde{\delta}_{max}, \tilde{\delta}^* \right), \tag{9}$$

where $\Delta \tilde{\sigma}_f = \Delta \sigma_f / \sigma_0$, $\sigma_0 = V_f \tau (L_f/d_f)/2$, V_f the fiber volume fraction, τ the interfacial frictional bond strength, L_f the fiber length, d_f the fiber diameter, $\Delta \tilde{\delta} = \Delta \delta/(L_f/2)$, $\tilde{\delta}_{max} = \delta_{max}/(L_f/2)$, $\tilde{\delta}^* = \delta^*/(L_f/2) = (2\tau L_f)/(E_f d_f)$, and E_f the fiber modulus. Normalized curves of fiber bridging stress-crack opening displacement relation for a short fiber composite with $\tilde{\delta}^* = 0.002$ are shown in Figs. 2 and 3 for pre-peak and post-peak respectively.

Monotonic bridging law due to fibers, $\sigma_f(\delta)$, is required, since δ_{max} is related to the maximum fiber bridging stress, $\sigma_{f\,max}$, in the preceding load cycle. The expression of $\sigma_f(\delta)$ is summarized in Appendix A, and more details can be found in Li [17].

The aggregate bridging law under cyclic and monotonic loading are also required in order to obtain $\Delta \sigma_b$ by superposition. The cyclic bridging law, $\Delta \sigma_m(\Delta \delta)$, is modeled with a simple assumption based on a monotonic bridging law, $\sigma_m(\delta)$ [18]. This empirical monotonic bridging law fits a wide range of experimental data. The cyclic bridging law assumes that the aggregate bridging stress, σ_m, and the crack opening displacement, δ, decrease to zero when unloading takes place.
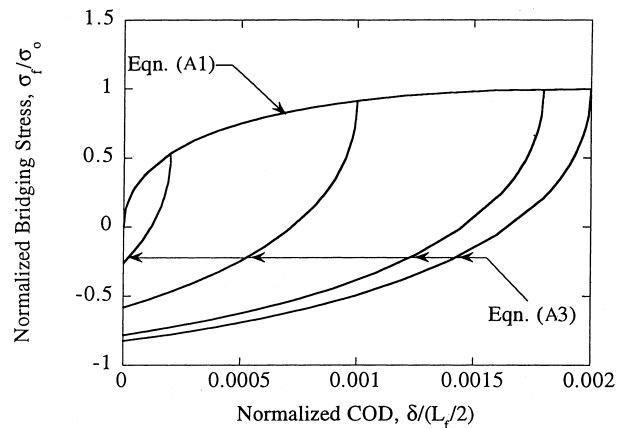

Fig. 2. Fiber bridging stress-crack opening displacement (COD) relation (bridging law) for pre-peak [7].
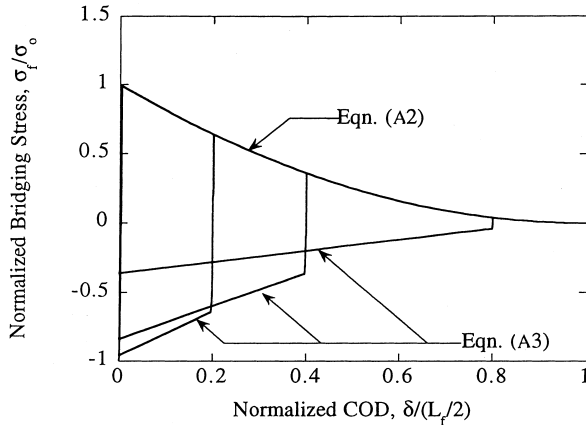
Fig. 3. Fiber bridging stress-crack opening displacement (COD) relation (bridging law) for post-peak [7].

The expressions of $\Delta\sigma_m(\Delta\delta)$ and $\sigma_m(\delta)$ are summarized in Appendix B.

2.3. Cycle-dependent degradation of crack bridging

Cycle-dependent degradation of crack bridging is shown to exist by experimental observations in fiber reinforced ceramic [19–21], fiber reinforced concrete [22], and concrete [23,24]. Degradation of fiber- and aggregate-matrix interface bond is the main mechanism when no fiber or aggregate rupture is observed. Based on this observation, a bilinear degradation function for fiber bridging is suggested by Matsumoto and Li [7].

As for the degradation of fiber bridging, the fiber-matrix interfacial frictional bond strength, τ, is assumed to change as follows:

$$\frac{\tau}{\tau_i} = \max \text{ of} \begin{cases} 1.0 + D_1 \sum_{i=1}^{N} \Delta\delta_i(x) \\ B + D_2 \sum_{i=1}^{N} \Delta\delta_i(x) \end{cases}, \qquad (10)$$

where τ_i is the initial bond strength, D_1 the degradation coefficient for the early trend (negative for degradation), $\Delta\delta_i$ the crack opening displacement change at ith cycle, B the intercept for the long trend, and D_2 the degradation coefficient for the long trend (negative for degradation). Here, the interfacial bond degradation is measured with

$$\sum_{i=1}^{N} \Delta\delta_i(x) = \text{accumulated crack opening displacement}$$

change at x, (11)

where x is the position on the crack surface. This parameter takes a value related to the number of cycles and the crack opening displacement change experienced at each point on the bridged crack surface. For a

growing crack with non-uniform crack profile, the parameter takes the maximum value near the crack mouth and the minimum at the crack tip, meaning that crack bridging degradation is the most severe near the crack mouth and minimal at the crack tip.

Similarly, as for the degradation of aggregate bridging, the current degraded aggregate bridging stress, σ_m, is scaled to the original undegraded aggregate bridging stress, σ_{m0}, with the accumulated crack opening displacement change, namely

$$\frac{\sigma_m}{\sigma_{m0}} = \max \text{ of} \begin{cases} 1.0 + D_{m1} \sum_{i=1}^{N} \Delta\delta_i(x) \\ B_m + D_{m2} \sum_{i=1}^{N} \Delta\delta_i(x) \end{cases}, \qquad (12)$$

where D_{m1} the degradation coefficient for the early trend (negative for degradation), B_m the intercept for the long trend, and D_{m2} = degradation coefficient for the long trend (negative for degradation).

Total degradation of crack bridging stress is obtained by the superposition of degrading bridging stress due to fibers and aggregates (Fig. 4).

3. Fatigue life analysis of FRCs

Fatigue life of one plain concrete and four different FRCs is simulated with the theoretical model summarized above and is represented in the form of the S–N diagram. A comparison of this theoretical diagram with the experimental one provides confidence in the overall approach of the model. First, the experiment by Zhang and Stang [25] is summarized. Second, the flow of fatigue life computation is explained. Finally, fatigue crack growth is compared between plain concrete and FRCs, and the theoretical diagram is shown and compared with the experimental one.
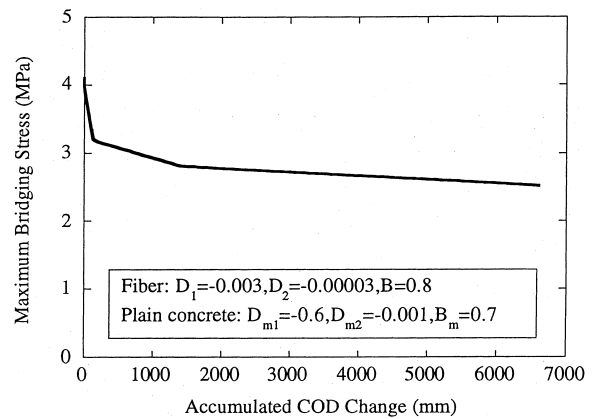

Fig. 4. Crack bridging degradation assumed in the current fatigue life analysis.

3.1. Experiment

The fatigue study carried out by Zhang and Stang included one plain concrete and four FRCs (hereafter referred to as PLC, SS1, HS1, HS2, and HYB) [25]. The concrete matrix is made of coarse aggregates of maximum size 8 mm and fine aggregates of maximum size 4 mm, and fiber volume fraction as shown in Table 1. The beams with depth 100 mm, thickness 50 mm, and length 350 mm were loaded in three point flexure with a span of 345 mm. In the monotonic flexural loading test, the modulus of rupture (σ_r) of each of the five materials was measured (Table 5). In the cyclic flexural loading test, constant amplitude load was applied, where the maximum load level varied from 75 to 95% of σ_r for PLC and HS2 and from 90 to 95% for SS1, HS1, and HYB. The minimum load level was always 20% of the maximum ($R = 0.2$). As a result of cyclic tests, the S–N diagram was obtained for the five materials (Figs. 16 and 17).

3.2. Flow of fatigue life computation

Flow of the theoretical fatigue life computation consists of two steps and is explained below (Fig. 5).

First, analysis is performed to compute the modulus of rupture of each material under monotonic loading. The theoretical model can compute the applied stress at which the crack is about to propagate for a given crack length between the initial flaw size, a_0, and the beam depth. Thus, the relation between the crack propagation stress and the crack length can be obtained, and this shows the maximum stress sustainable throughout the crack growth under monotonic flexural loading, which is the modulus of rupture of that material. The relation is specific to each material, since crack bridging is dependent on the presence, type, and amount of bridging fibers. The relation also determines the initial size of the fatigue crack, a_i, in Eq. (2). For example, fatigue loading at 80% of σ_r implies that the crack has grown at first loading to its corresponding crack length, a_i, and continues to grow throughout the following cyclic loading (Fig. 5).

Second, analysis is performed to compute the fatigue life of each material under cyclic loading. Starting from the initial fatigue crack size, a_i, ΔK_{tip} and K_{max} are computed for a crack length, a, under a given constant stress amplitude. With $\Delta K_{tip}(a)$ known, $N(a)$ can be
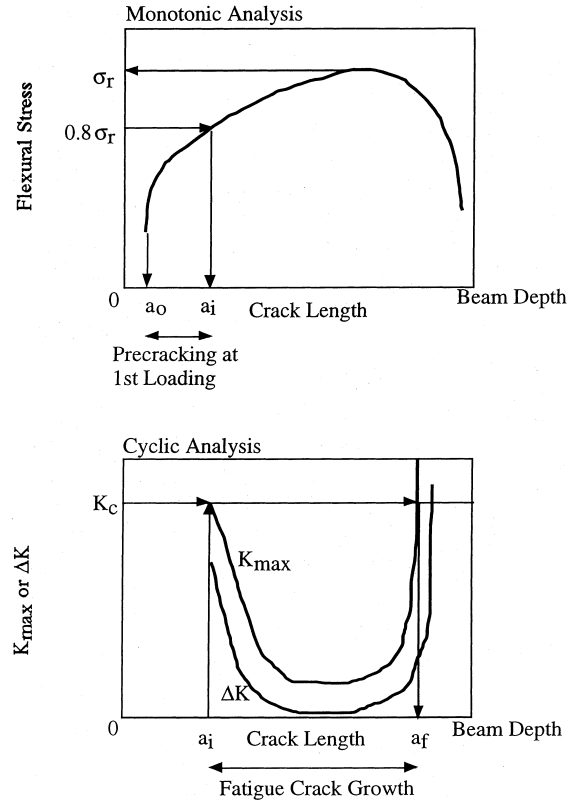

Fig. 5. Flow of monotonic and cyclic analysis.

calculated with the use of Eq. (2). Crack bridging degradation effect is considered as described in the previous section, and this becomes prominent, as the crack becomes longer and the number of cycles becomes larger. Fatigue life is defined by the number of cycles at which the maximum stress intensity factor, K_{max}, surpasses the matrix fracture toughness, K_c. Physically this means that materials fail when unstable fracture takes place.

3.3. Theoretical analysis

The monotonic analysis is applied to compute the modulus of rupture of the five materials with microstructural parameters as shown in Tables 1–4. The parameters have been measured independently of this theoretical work, except for matrix fracture toughness and initial flaw size. For all five materials, the matrix fracture toughness is assumed to be 0.5 MPa$\sqrt{m}$ [26],

Table 1
Mix compositions [25]

	PLC	SS1	HS1	HS2	HYB
Smooth steel V_f (%)	0	1	0	0	0
Hooked-end steel V_f (%)	0	0	1	2	1
Polypropylene V_f (%)	0	0	0	0	1

Table 2
Fiber parameters [25]

Fiber	d_f (μm)	L_f (mm)	E_f (GPa)
Smooth steel	400	25	210
Hooked-end steel	500	30	210
Polypropylene	48	12	12

Table 3
Matrix parameters [22] (*: assumed value)

Matrix	E_m (GPa)	σ_m^u (MPa)	p	δ_0 (mm)	K_c (MPa $\sqrt{m}$)
	35	5.4	1.2	0.015	0.5*

Table 4
Interface parameters [27,28]

Interface	SS1	HS1	HS2	HYB (hook-end steel, polypropylene)
τ_0 (MPa)	6.0	4.5	4.5	4.5, 0.8
a_1 (MPa/mm)	–4.0	–2.0	–2.0	–2.0, 0.0
f	0.8	0.75	0.75	0.75, 0.0

and the initial flaw size, a_0, is assumed to exist with the size of 3 mm on the tension face of the beam in order to account for the most severe situation of a flexural beam with a flaw.

Slip-softening relation at the fiber-matrix interface under monotonic loading is used and is assumed to take the simple form

$$\tau(\delta) = \begin{cases} \tau_0 & \text{for } \delta \leqslant \delta^* \\ \tau_0 + a_1\delta & \text{for } \delta^* < \delta \end{cases}, \quad (13)$$

where τ_0 is the initial bond strength and a_1 the slip-softening/hardening coefficient (negative for softening). The values of τ_0 and a_1 are shown in Table 4. These values for HS1, HS2, and HYB are obtained from experimental evaluations on the same concrete mix, and those for SS1 are chosen based on typically observed values [27,28].

The resulting theoretical relation between the crack propagation stress and the crack length is shown for all five materials in Fig. 6, and the theoretical σ_r is summarized in Table 5. It is shown that σ_r is improved by the addition of fibers and that the crack length at σ_r varies from one to another. For example, the σ_r of HS2 is exerted at a long crack length (0.07 m), while the σ_r of
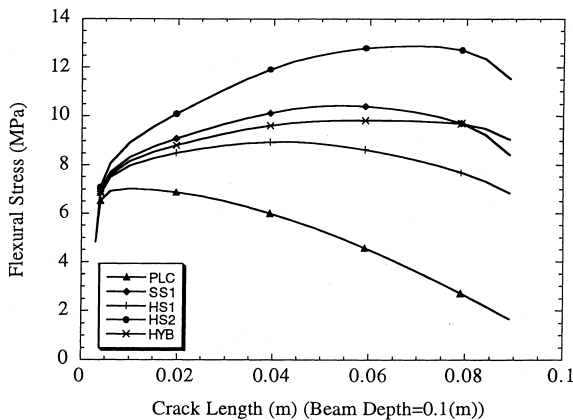

Fig. 6. Monotonic analysis: crack length vs. equilibrium flexural stress.

Table 5
Experimental and theoretical σ_r

	PLC	SS1	HS1	HS2	HYB
Experimental σ_r [25] (MPa)	6.94	10.15	8.88	12.82	9.46
Theoretical σ_r (MPa)	7.02	10.43	8.95	12.9	9.83

PLC takes place at a short crack length (0.006 m). This is because the modulus of rupture of HS2 is mainly attributed to the sustainable stress increase due to crack bridging after first cracking, while the one of PLC relies mainly on the stress increase before first cracking. Other three FRCs (SS1, HS1, and HYB) show similar results, falling between PLC and HS2, and no significant effect of additional 1% of polypropylene fibers is observed in HYB when compared to the effect of additional 1% of hooked-end steel fibers in HS2. In the monotonic analysis, the theoretical values of σ_r agree well with the experimentally measured ones.

The cyclic analysis needs some additional parameters. First, Paris law constants are needed. These constants have not been well determined for cementitious materials, although experimental investigations have been conducted by four independent research groups [9–13]. Paris constant, n, varies from 3.12 to 14.0 for concrete [9,12] and from 2.31 to 4.18 for mortar [13], depending on mixes and loading conditions. The current analysis assumes that the Paris law constants measured by Baluch et al. [9] (Table 6) applies to the matrix of FRCs. These Paris law constants were measured under $R = 0.2$ which is the same ratio used in the fatigue experiment by Zhang and Stang [25], and, with these constants, the cyclic analysis is performed under $R = \sigma_{min}/\sigma_{max} = 0.2$.

Second, the degradation coefficients (D_1, D_2, and B) and (D_{m1}, D_{m2}, and B_m) are determined as follows (Tables 7 and 8). For the plain concrete, the set of degradation coefficients (D_{m1}, D_{m2}, and B_m) shown in Table 7 is estimated to yield a close agreement with the experimental S–N diagram for plain concrete, and this set of coefficients for aggregate bridging is also used for the four FRCs. Thus, two kinds of degrading crack bridging

Table 6
Paris law constants [9]

Paris constant	C	n
	9.03×10^{-6}	3.12

Table 7
Degradation coefficients for aggregate bridging

	PLC
D_{m1} (/mm)	–0.6
D_{m2} (/mm)	–0.001
B_m	0.7

Table 8
Degradation coefficients for interface bond strength

	SS1	HS1	HS2	HYB (hooked-end steel, polypropylene)
D_1 (/mm)	−0.003	−0.003	−0.003	−0.003, −0.003
D_2 (/mm)	−0.00003	−0.00003	−0.00003	−0.00003, −0.00003
B	0.8	0.8	0.8	0.8, 0.8

stresses are superposed in the case of FRCs. For the four different FRCs, only one set of interfacial bond degradation coefficients (D_1, D_2, and B) is used to yield a general agreement with the experimental S–N diagrams of all the FRCs, regardless of the type and amount of fibers in a material. No attempt is made to estimate a set of degradation coefficients for each FRC. This is because there is a lack of experimental data for any of the four FRCs and because, except for the polypropylene fiber, the interface degradation is considered to be on the same order for the same kind of steel fiber-cement matrix interface in both of the smooth and hooked-end steel fiber reinforced concrete.

Although typically observed microstructural parameters are used when they are not available for a given FRC, future experimental investigations are needed for the determination of those parameters in order to perform fatigue crack growth and fatigue life analysis in a more consistent manner.

3.4. Results

Fatigue crack growth behavior of plain concrete and four FRCs is shown in Figs. 7–11. A theoretical S–N diagram is shown in Figs. 16 and 17.

Fatigue crack growth has been observed to show three stages: initial decelerated growth, steady state growth, and final accelerated growth [29]. These three
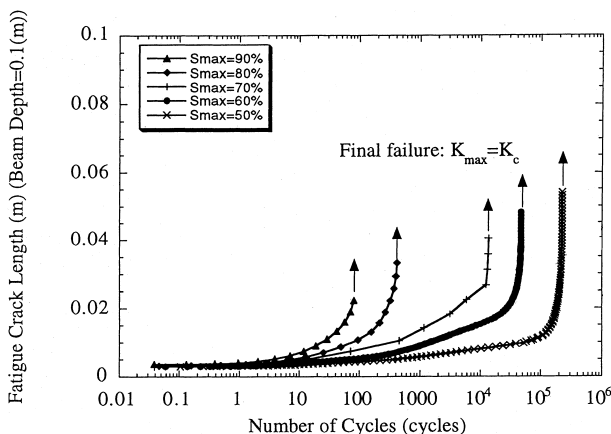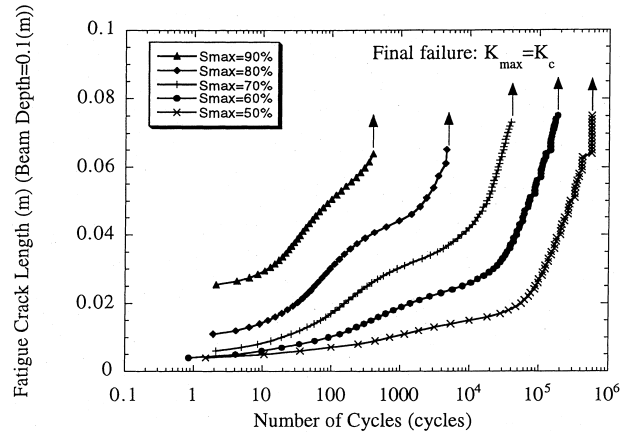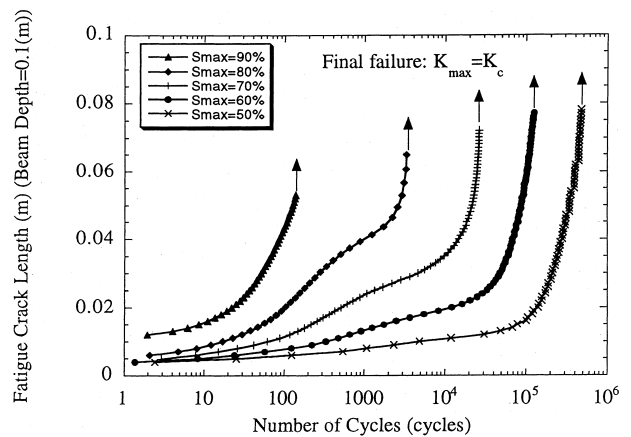

Fig. 8. Fatigue crack growth in smooth steel 1% FRC (SS1).

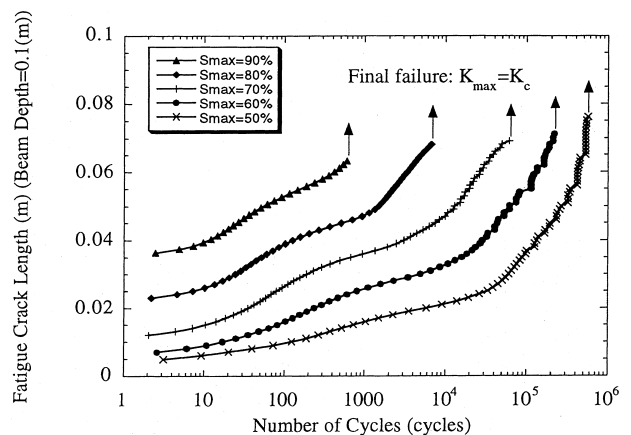Fig. 9. Fatigue crack growth in hooked-end steel 1% FRC (HS1).

Fig. 10. Fatigue crack growth in hooked-end steel 2% FRC (HS2).

Fig. 7. Fatigue crack growth in plain concrete (PLC).

stages are caused by the changes of the total crack tip stress intensity factor amplitude, ΔK_{tip}, which is the sum of the positive term, ΔK_a, and the negative term, ΔK_b, in Eq. (4). ΔK_{tip} decreases when $|\Delta K_b|$ increases due to the
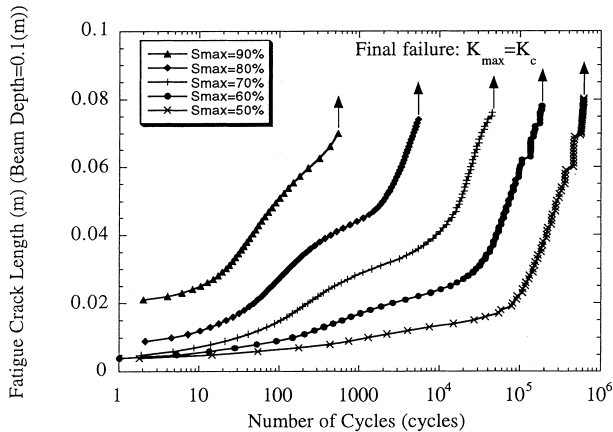
Fig. 11. Fatigue crack growth in hooked-end steel 1% + polypropylene 1% FRC (HYB).

initial development of the bridging zone, holds a constant value when the increase of ΔK_a due to the crack length increase is balanced with the increase of $|\Delta K_b|$, and eventually increases as the crack approaches the specimen boundary (due to rapid increase in ΔK_a). These three changes correspond to the experimentally observed three stages of fatigue crack growth. Then, final failure takes place by unstable crack propagation, whenever the crack tip stress intensity factor at the maximum load level, K_{max}, reaches the matrix fracture toughness, K_c. Arrows in Figs. 7–11 represent the final unstable crack propagation at corresponding final crack length.

Fatigue crack growth behavior of plain concrete is distinct from that of other four FRCs (Fig. 7). From the monotonic analysis, the initial fatigue crack length, a_i, is about 3 mm for all cyclic load amplitudes employed ($S_{max} = \sigma_{max}/\sigma_r$ and $R = \sigma_{min}/\sigma_{max} = 0.2$), and, from the cyclic analysis, the final fatigue crack length, a_f, ranges between 22 and 54 mm. The fatigue crack development is limited to below 54 mm, nearly the half of the beam depth, and the crack growth is prominent in the final acceleration stage and not significant in the initial deceleration and steady state stage. This is because of the bridging zone size in plain concrete, which is smaller than that of FRCs, becomes fully developed at a shorter crack length. The reduction of the total ΔK_{tip} cannot be expected as the crack continues to elongate further, leading the crack to transit from decelerated crack growth to accelerated crack growth.

Fatigue crack growth behavior of FRCs varies depending on the type of fiber reinforcement and stress level as seen in Figs. 8–11. However, there are two general trends that discern FRCs from plain concrete. First, longer fatigue cracks develop over the beam depth. The initial crack length, a_i, ranges between 4 and 35 mm depending on the cracking at different levels of

first loading, and the final crack length, a_f, is above 50 mm for all cases. Second, the initial crack growth deceleration is observed over a large range of initial crack length increase. For example, hooked-end steel 2% FRC has a_i ranging between 6 and 35 mm and a_f between 63 and 76 mm (Fig. 10). The initial crack growth deceleration is prominent in this FRC. As a result, large fatigue crack development is seen in the initial 10% of fatigue life. In general, fatigue crack growth curves of FRCs and plain concrete can be classified into three groups in the same way as crack propagation curves under monotonic loading. SS1, HS1, and HYB show a similar fatigue crack growth, while PLC and HS2 show remarkable accelerated and decelerated growth respectively. No significant difference between 1% steel FRCs (SS1 and HS1) arises, and, again, no significant effect of additional 1% of polypropylene fibers is observed in HYB when compared to the effect of additional 1% of hooked-end steel fibers in HS2.

The effect of fiber volume fraction increase from 1 to 2% can be seen in Figs. 9 and 10, and the behavior of fatigue crack growth and crack mouth opening displacement (CMOD) distinctly changes with this additional 1% of fiber volume fraction. First, the initial crack length, a_i, which is caused by the first load application and from which the fatigue crack starts to elongate is significantly long for HS2. The initial crack length of HS2 ranges from 5 to 36 mm, while that of HS1 ranges from 4 to 12 mm. This happens because HS2 is loaded well above the first cracking load for the maximum load ranging from 50 to 90% of σ_r which is exerted at a long crack length due to the large increase of the sustainable stress after first cracking (Fig. 6). Second, the fatigue cracks grow rather steadily throughout the fatigue life in HS2, while, in HS1, they propagate rapidly just before the final failure, and the onset of the final rapid growth can be identified. For example, the fatigue crack length of HS2 at 10% of its fatigue life, 0.1 N_f, under each S_{max} ranges from 29 to 50 mm, while that of HS1 ranges from 13 to 17 mm. This means that HS2 loaded under $S_{max} = 90\%$ grows the crack from 36 to 50 mm during 0.1 N_f and spends the rest of its life, 0.9 N_f, with the fatigue crack longer than 50 mm.

The two differences mentioned above are seen also in Figs. 12 and 13. When the five materials are compared in terms of crack length and mouth opening displacement under the same stress ratio to σ_r ($S_{max} = 0.9$ and $R = 0.2$), the crack of HS2 starts as the longest and widest among the five materials and stays so for the most of its fatigue life. However, under the same stress magnitude for all materials ($\sigma_{max} = 6.3$ MPa $= 90\%$ of plain concrete's σ_r and $R = 0.2$), the crack of HS2 is certainly the shortest and narrowest throughout the fatigue life, while providing the longest fatigue life (Figs. 14 and 15). This comparison between two
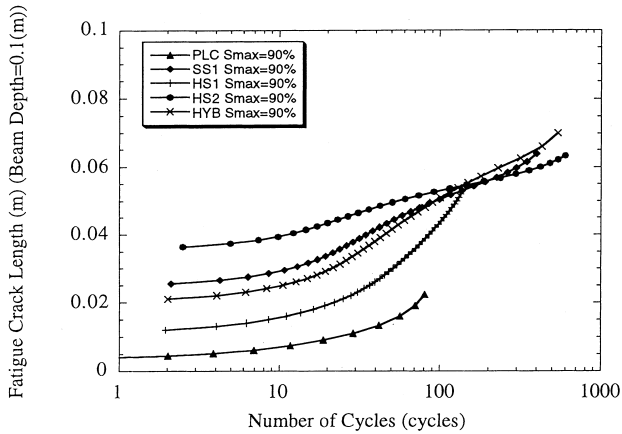
Fig. 12. Fatigue crack growth behavior of plain concrete and four FRCs under $S_{max} = 90\%$ and $R = 0.2$.
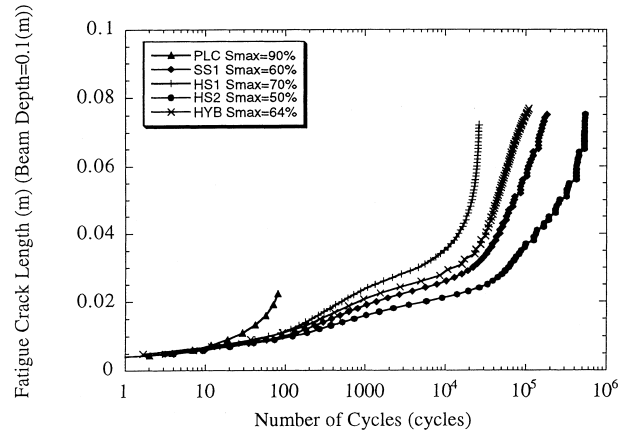

Fig. 14. Fatigue crack growth behavior of plain concrete and four FRCs under $\Delta\sigma = 5.0$ MPa and $R = 0.2$.

different fiber volume fractions implies that high stress ratio application has to be limited by an acceptable value of CMOD under service conditions, when high strength FRCs are utilized for higher loads than plain concrete. This is due to the fact that increased environmental attacks are expected for a wider crack [30–32]. Details of CMOD analysis can be found elsewhere [33].

The theoretical S–N diagrams in Figs. 16 and 17 can be readily constructed with the number of cycles to failure shown in Figs. 7–11 and are compared to the experimental S–N diagrams.

The theoretical results agree well with the experimental ones for two materials: plain concrete and hooked-end steel 2% FRC. The theoretical fatigue life for plain concrete agrees with the experimentally measured life at three of the higher load levels (90, 80, and 70% of σ_r), with deviation at the lower load levels (60 and 50%). Similarly, the theoretical fatigue life for hooked-end steel 2% FRC agrees with the experimentally measured life at two load levels (80 and 75% of σ_r),
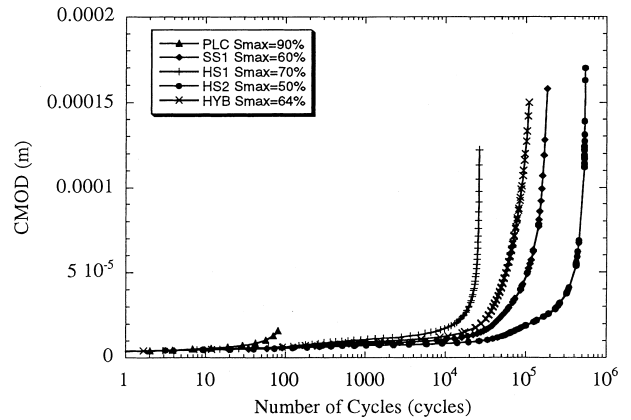

Fig. 15. CMOD behavior of plain concrete and four FRCs under $\Delta\sigma = 5.0$ MPa and $R = 0.2$.
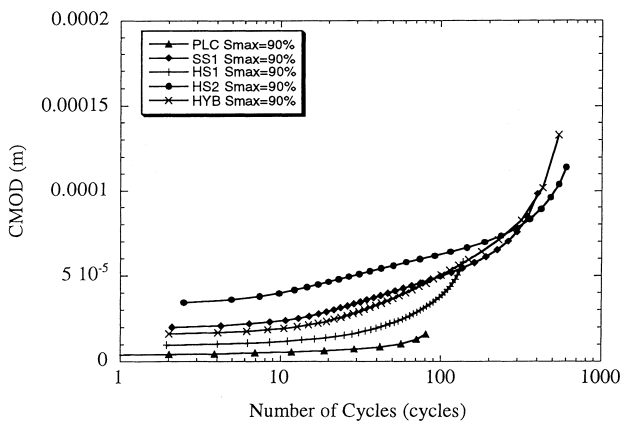

Fig. 13. CMOD behavior of plain concrete and four FRCs under $S_{max} = 90\%$ and $R = 0.2$.
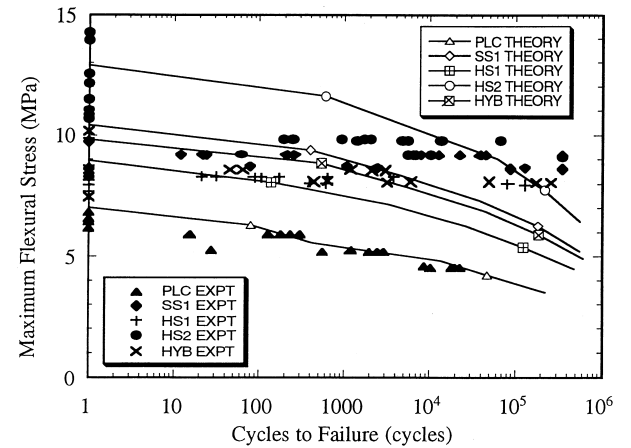

Fig. 16. Theoretical S–N diagram and experimental data [25] of plain concrete and four FRCs.
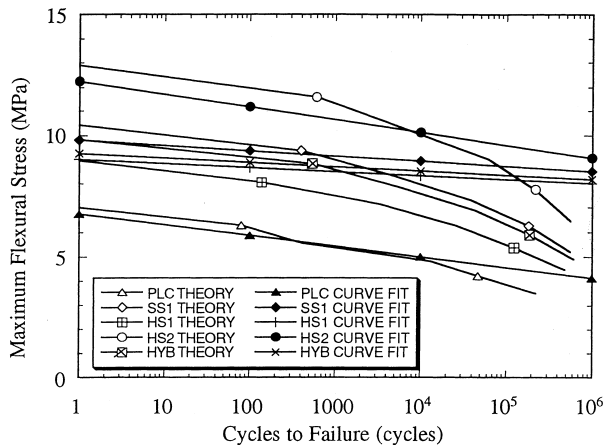
Fig. 17. Theoretical S–N diagram and curve fit to experimental data [25] of plain concrete and four FRCs.

although the theoretical S–N relation deviates from experimental data for the higher (90%) and lower (60 and 50%) load levels. However, the theoretical S–N relation for other three FRCs (SS1, HS1, and HYB) deviates far from the corresponding experimental data. While the theoretical relation shows the fatigue strength decline to 50% of σ_r at 5–7×10^5 cycles, experimental data shows that the fatigue strength is about 90% of σ_r at 10^6 cycles.

Two salient discrepancies are noted in comparison of theoretical results with experimental data. First, the theoretical S–N relation of plain concrete and hooked-end steel 2% FRC is somewhat deviant from the straight line curve fit to experimental data. Second, the theoretical S–N relation of the other three FRCs does not agree with the curve fitting result.

The first discrepancy may arise because of either one of the following two reasons. First, the assumption of Paris law for crack growth rate may not be correct near the upper and lower limit. Crack growth rate is very high near the upper limit of matrix fracture toughness, K_c, while it is negligible near the lower limit of fatigue threshold, ΔK_{th}. Experimentally, fast crack growth has been observed in plain concrete when the maximum level of cyclic loading is half of σ_r, and no crack growth at one fourth [9]. This correction would decrease the fatigue life at high load level and increase it at low load level, resulting in a theoretical S–N relation closer to the straight line curve fit to experimental data. Second, the assumed functions of crack bridging degradation, (10) and (12), may not be accurate enough for various load levels, since the current function does not take into account the effect of initial crack opening displacement which is different for a different load level. This means that there is no distinction between a large number of small opening changes and a small number of large opening changes, when both cases amount to the same accumulated crack opening displacement change. This

correction would again increase the fatigue life at low load level. Despite the fact that these two reasons are plausible, whether or not the S–N relation is a straight line on a semi log plot remains a question. The S–N relation has to be determined experimentally with statistically enough number of data points and with accurate representation in a mathematical form.

The second significant discrepancy may be explained as follows. In the S–N diagram, there is a lack of experimental data for lower load levels. The experimental fatigue life for the three FRCs is measured at 90–95% of σ_r. As a result, the fatigue life measurement can be easily distributed over a broad range, since this high load level is within the variability range of σ_r (see data on y-axis in Fig. 16). This leads to the seemingly high fatigue strength mentioned above for the three FRCs, which is contrary to the theoretical fatigue strength. Also, fatigue strength of FRCs has been reported to be within 40–70% of σ_r [34–38], and there is only one report for above 90% of σ_r [39]. The two corrections for the first discrepancy apply here as well, and again the S–N relation needs to be determined for lower load levels with statistical confidence in order to make fair comparisons. It should be noted that the current theoretical model applies to any given FRC with friction controlled fiber-matrix interface, if all the microstructural parameters shown in Tables 1–4 and Tables 6–8 are available for the model. These microstructural parameters for the five materials in this study are typically observed values that have been obtained from several independent measurements by other researchers [9,22,25,27,28] and used in the theoretical analysis.

4. Conclusions

Fatigue crack growth for plain concrete and four different FRCs has been simulated with a fracture mechanics based model. The four FRCs show that long fatigue cracks develop over the beam depth at final failure and that their initial crack growth is decelerated over a large range of initial crack length increase. These two differences discern the behavior of FRCs from plain concrete. Furthermore, under the same stress ratio, it is shown that, compared to hooked-end steel 1% FRC, hooked-end steel 2% FRC shows a less catastrophic failure with slower crack growth towards the final failure, but that it develops a longer and wider fatigue crack in the beginning of the fatigue life. This implies that high stress ratio application to a high fiber volume FRC should be limited by an acceptable CMOD value under service conditions in order to minimize environmental damage resulting due to cracking.

Theoretical S–N diagrams have been made for the five materials and compared with experimental S–N

diagrams. The theoretical results agree well with the experimental ones for plain concrete and hooked-end steel 2% FRC, while they do not agree with that for smooth steel 1% FRC, hooked-end steel 1% FRC, and hooked-end 1% + polypropylene 1% FRC. The disagreement could be possibly removed by refining the three aspects of crack bridging degradation function. First, crack bridging degradation could be different for steel and polypropylene fiber. Steel fibers suffer from interfacial bond degradation, while polymeric fibers could be subjected to fiber fatigue rupture. Second, among steel fibers, a different set of degradation coefficients is appropriate depending on the combination of fiber and matrix. Third, for both of above two aspects, the function of crack bridging degradation has to be dependent on initial crack opening displacement as well. An increase in the knowledge on fatigue life of FRCs may be attained with further refinement of the theoretical model, in conjunction with more accurate experimental S–N diagrams.

Crack growth of plain concrete and four FRCs under monotonic loading has been analyzed in conjunction with fatigue crack growth. The resulting relations between crack propagation stress and crack length yield a close prediction on the modulus of rupture for five materials, and it also indicates the crucial role of bridging zone development in the crack wake under monotonic and cyclic loading.

The theoretical results show that a single set of degradation parameters explains qualitatively a wide range of experimental fatigue life data. Further, improvement of fatigue life of FRCs necessitates a focus on the fiber-matrix interface degradation. Degradation of crack bridging has to be minimized with the understanding of degradation mechanisms. Such an experimental study can be executed effectively in conjunction with the theoretical analysis presented in this paper in order to contribute to the efficient development of high fatigue resistant FRC.

Acknowledgements

Appendix A. Monotonic and cyclic fiber bridging law

A.1. Monotonic fiber bridging law

The monotonic fiber bridging law, $\sigma_f(\delta)$, is given in a normalized form derived by Li [17]. For pre-peak part,

$$\tilde{\sigma}_f\left(\tilde{\delta}\right) = g\left[2\left(\frac{\tilde{\delta}}{\tilde{\delta}^*}\right)^{1/2} - \left(\frac{\tilde{\delta}}{\tilde{\delta}^*}\right)\right] \qquad \text{for } 0 \leqslant \tilde{\delta} \leqslant \tilde{\delta}^*,$$

(A.1)

where $\tilde{\sigma}_f = \sigma_f/\sigma_0$, $\sigma_0 = V_f\tau(L_f/d_f)/2$, V_f the fiber volume fraction, τ the interfacial frictional bond strength, L_f the fiber length, d_f the fiber diameter, $g = 2/(4+f^2)$ $(4+f^2)(1+e^{\pi f/2})$, f the snubbing coefficient, $\tilde{\delta} = \delta/(L_f/2)$, $\tilde{\delta}^* = \delta^*/(L_f/2) = (2\tau L_f)/(E_f d_f)$, and E_f the fiber modulus.

For post-peak part,

$$\tilde{\sigma}_f\left(\tilde{\delta}\right) = g\left[1 - \left(\tilde{\delta} - \tilde{\delta}^*\right)\right]^2 \qquad \text{for } \tilde{\delta}^* < \tilde{\delta} \leqslant 1. \qquad (A.2)$$

A.2. Cyclic fiber bridging law

The cyclic fiber bridging law, $\Delta\sigma_f(\Delta\delta)$, was modeled by Matsumoto and Li [40] and is given in a normalized form by

$$\Delta\tilde{\sigma}_f\left(\Delta\tilde{\delta}\right) = \begin{cases} \Delta\tilde{\sigma}_f\big|_{\text{prepeak}} & \left(\text{for } 0 \leqslant \tilde{\delta} \leqslant \tilde{\delta}^*\right) \\ \Delta\tilde{\sigma}_f\big|_{\text{postpeak}} & \left(\text{for } \tilde{\delta}^* < \tilde{\delta} \leqslant 1\right) \end{cases}, \qquad (A.3)$$

where $\Delta\tilde{\sigma}_f = \Delta\sigma_f/\sigma_0$ and $\Delta\tilde{\delta} = \Delta\delta/(L_f/2)$.

For pre-peak part,

$$\Delta\tilde{\sigma}_f\big|_{\text{prepeak}} = g\left[2\sqrt{2}\left(\frac{\Delta\tilde{\delta}}{\tilde{\delta}^*}\right)^{1/2}\left(1 - \tilde{\delta}_{\max}\right) - \frac{\Delta\tilde{\delta}}{\tilde{\delta}^*} \right.$$
$$\left. + \sqrt{2}\left(\frac{\Delta\tilde{\delta}}{\tilde{\delta}^*}\right)^{3/2}\tilde{\delta}^* - \frac{1}{2}\left(\Delta\tilde{\delta}\right)^2\right], \qquad (A.4)$$

where $\tilde{\delta}_{\max} = \delta_{\max}/(L_f/2)$ and $\delta_{\max} = $ maximum crack opening displacement experienced in the preceding load cycle.

For post-peak part, there are two stages. When only some fibers are in sliding back into matrix ($\beta \leqslant \beta_0$), the bridging law, $\Delta\tilde{\sigma}_f\big|_{\text{postpeak}}$, is the same as that of pre-peak part and is given by Eq. (A.4) for $\beta \leqslant \beta_0$ where $\beta = \Delta\tilde{\delta}/\tilde{\delta}_{\max}$ and

$$\beta_0 = \left(\frac{\sqrt{\frac{\tilde{\delta}_{\max}}{2\tilde{\delta}^*}} - \sqrt{\frac{\tilde{\delta}_{\max}}{2\tilde{\delta}^*} - 2\tilde{\delta}_{\max}\left(1 - \tilde{\delta}_{\max}\right)}}{\tilde{\delta}_{\max}}\right)^2. \qquad (A.5)$$

When all fibers are in sliding back into matrix, the bridging law, $\Delta\tilde{\sigma}_f\big|_{\text{postpeak}}$, is given by

$$\Delta\tilde{\sigma}_f\Big|_{\text{postpeak}} = g\Big[2\Big(1 - \tilde{\delta}_{\max}\Big)$$
$$\times \Big(1 - \tilde{\delta}_{\max} + \Delta\tilde{\delta}\Big)\Big] \qquad \text{for } \beta_0 < \beta.$$
$$(A.6)$$

Appendix B. Monotonic and cyclic aggregate bridging law

The monotonic aggregate bridging law is given by an empirical equation proposed by Stang [18]. The aggregate bridging stress, σ_m, as a function of the crack opening displacement, δ, is given by

$$\sigma_m(\delta) = \frac{\sigma_m^u}{1 + (\delta/\delta_0)^p}, \qquad (B.1)$$

where $\sigma_m^u = $ maximum aggregate bridging stress at $\delta = 0$, δ_0 the crack opening displacement which corresponds to the half of σ_m^u, and p describes the shape of the bridging curve.

The cyclic aggregate bridging law follows a typical formulation where stress and strain return to the origin upon unloading [41], and this is simply given by

$$\Delta\sigma_m(\Delta\delta) = \frac{\sigma_{m\max}}{\delta_{\max}}\Delta\delta, \qquad (B.2)$$

where $(\delta_{\max}, \sigma_{m\max})$ is the point at which unloading occurs.

References

[1] Rizkalla SH, Mufti AA. Recent innovation for concrete highway bridges. In: Chong KP, editor. Proceedings of the ASCE 4th Materials Engineering Conference, 1996:1063–1071.

[2] Shirazi HH, Rasoulian M, King B. Design and construction of a bonded fiber concrete overlay of CRCP. In: Chong KP, editor. Proceedings of the ASCE 4th Materials Engineering Conference, 1996:1647–658.

[3] Strand D, MacDonald CN, Ramakrishnan V, Rajpathak VN. Construction applications of polyolefin fiber reinforced concrete. In: Chong KP, editor. Proceedings of the ASCE 4th Materials Engineering Conference, 1996:103–12.

[4] Krstulovic-Opara N, Haghayeghi AR, Haidar M, Krauss PD. Use of conventional and high-performance steel-fiber reinforced concrete for bridge deck overlays. ACI Materials Journal 1995:92(6):669–77.

[5] Balaguru PN, Shah SP. Fiber-Reinforced Cement Composites. New York: McGraw-Hill, 1992.

[6] Li VC, Matsumoto T. Fatigue crack growth analysis of fiber reinforced concrete with effect of interfacial bond degradation. Journal of Cement and Concrete Composites 1998:20(5):339–51.

[7] Matsumoto T, Li VC. Uniaxial cyclic behavior of discontinuous fiber reinforced composites. In: Chong KP, edtior. Proceedings of the ASCE 4th Materials Engineering Conference, 1996:426–35.

[8] Wu HC, Matsumoto T, Li VC. Buckling of bridging fibres in composites. Journal of Materials Science Letters 1994:13:1800–803.

[9] Baluch MH, Qureshy AB, Azad AK. Fatigue crack propagation in plain concrete. In: Shah SP, Swartz SE, editors. Proceedings of the SEM/RILEM International Conference on Fracture of Concrete and Rock, 1987:80–87.

[10] Bazant ZP, Xu K. Size effect in fatigue fracture of concrete. ACI Materials Journal 1991:88(4):390–99.

[11] Bazant ZP, Schell WF. Fatigue fracture of high-strength concrete and size effect. ACI Materials Journal 1993:90(5):472–78.

[12] Perdikaris PC, Calomino AM. Kinetics of crack growth in plain concrete. In: Shah SP, Swartz SE, edtiors. Proceedings of the SEM/RILEM International Conference on Fracture of Concrete and Rock, 1987:64–69.

[13] Toumi A, Bascoul A, Turatsinze A. Crack progapation in concrete subjected to flexural-cyclic loading. Materials and Structures 1998:31:451–58.

[14] Paris PC, Erdogan F. A critical analysis of crack propagation laws. Journal of Basic Engineering 1963:85:528–34.

[15] Tada H. The Stress Analysis of Cracks Handbook. Paris Prod., 1985.

[16] Cox BN, Marshall DB. Stable and unstable solutions for bridged cracks in various specimens. Acta Metallurgica et Materialia 1991:39(4):579–89.

[17] Li VC. Postcrack scaling relations for fiber reinforced cementitious composites. Journal of Materials in Civil Engineering 1992:4(1):41–57.

[18] Stang H. Evaluation of properties of cementitious fiber composite materials. In: Reinhardt HW, Naaman AE, editors. Proceedings of the International RILEM/ACI Workshop, High Performance Fiber Cement Composites, 1992:388–406.

[19] Evans AG, Zok FW, McMeeking RM. Fatigue of ceramic matrix composites. Acta Metallurgica et Materialia 1995:43(3):859–75.

[20] Zok FW, McNulty J, Du ZZ, Evans AG. Effects of interfacial wear on fatigue failure in fiber reinforced CMCs. In: Proceedings of the International Conference on Composites Engineering-ICCE/1, 1994:597–98.

[21] Evans AG. Design and life prediction issues for high-temperature engineering ceramics and their composites. Acta Materialia 1997:45(1):23–40.

[22] Zhang J, Stang H. Experimental study on bridging stress of fiber reinforced concrete under uniaxial fatigue tensile load, in preparation.

[23] Hordijk DA, Reinhardt HW. Growth of discrete cracks in concrete under fatigue loading. In: Shah SP, editor. Proceedings of the NATO Advanced Research Workshop-Toughening Mechanisms in Quasi-Brittle Materials, 1990:553–68.

[24] Reinhardt HW, Cornelissen HAW, Hordijk DA. Tensile tests and failure analysis of concrete. Journal of Structural Engineering 1986:112:(11):2462–477.

[25] Zhang J, Stang H. Fatigue performance in flexure of fiber reinforced concrete. ACI Materials Journal, accepted for publication.

[26] Li VC, Mishra DK, Wu HC. Matrix design for pseudo-strain-hardening fibre reinforced cementitious composites. Materials and Structures 1995:28:586–95.

[27] Li VC, Stang H. Interface property characterization and strengthening mechanisms in fiber reinforced cement based composites. Journal of Advanced Cement Based Composites 1997:6(1):1–20.

[28] Li VC, Stang H, Krenchel H. Micromechanics of crack bridging in fiber reinforced concrete. Materials and Structures 1993:26:486–94.

[29] Stang H, Zhang J. Experimental determination of fatigue crack growth in fiber reinforced concrete. In: Silva Gomez JF et al., edtiors. Recent Advances in Experimental Mechanics, 1994:1347–52.

[30] Li VC. Performance driven design of fiber reinforced cementitious composites. In: Swamy RN, editor. Proceedings of the 4th

RILEM International Symposium on Fiber Reinforced Concrete 1992:12–30.

[31] Keer JG, Xu G, Filip R. Cracking and moisture penetration in fibre cement sheeting. In: Swamy RN, Barr B, editors. Fibre Reinforced Cements and Concretes-Recent Developments, 1989:592–601.

[32] Tsukamoto T. Tightness of Fiber Concrete. Darmstadt Concrete 1990:5:215–25.

[33] Matsumoto T. Fracture Mechanics Approach to Fatigue Life of Discontinuous Fiber Reinforced Composites. Ph. D. Thesis, The University of Michigan, Ann Arbor, 1998.

[34] Butler JE. The performance of concrete containing high proportions of steel fibres with particular reference to rapid flexural and fatigue loadings. In: Swamy RN, Barr B, edtiors. Fiber Reinforced Cements and Concretes-Recent Developments, 1989:544–52.

[35] Wu GY, Shivaraj SK, Ramakrishnan V. Flexural, Fatigue Strength, Endurance Limit, and Impact Strength of Fiber Reinforced Refractory Concretes. In: Swamy RN, Barr B, editors. Fiber Reinforced Cements and Concretes-Recent Developments, 1989:261–73.

[36] Vondran GL, Nagabhushanam M, Ramakrishnan V. Fatigue strength of polypropylene fiber reinforced concretes. In: Swamy RN, Barr B, editors. Fiber Reinforced Cements and Concretes Recent Developments, 1989:533–43.

[37] Ramakrishnan V, Gollapudi S, Zellers R. Performance characteristics and fatigue strength of polypropylene fiber reinforced concrete. In: Fiber Reinforced Concrete Properties and Applications SP-105, 1987:159–77.

[38] Ramakrishnan V, Lokvik BJ. Flexural fatigue strength of fiber reinforced concretes. In: Reinhardt HW, Naaman AE, editors. High Performance Fiber Reinforced Cement Composites, 1992:271–87.

[39] Ramakrishnan V, Josifek C. Performance characteristics and flexural fatigue strength of concrete steel fiber composites. In Proceedings of the International Symposium on Fiber Reinforced Concrete, 1987:2.73–2.84.

[40] Matsumoto T, Li VC. Crack bridging in discontinuous fiber reinforced composites under cyclic loading, in preparation.

[41] Horii H, Okui Y. Thermomechanics and micromechanics-based continuum theory for localization phenomena. In: Baker G, Karihaloo BL, editors. Proceedings of the International Union of Theoretical and Applied Mechanics (IUTAM) Symposium on Fracture of Brittle, Disordered Materials: Concrete, Rock and Ceramics, 1993:391–405.